*Reprinted from :*

NORTH-HOLLAND PUBLISHING COMPANY — AMSTERDAM

NUCLEAR INSTRUMENTS AND METHODS 150 (1978) 483-496 ; © NORTH-HOLLAND PUBLISHING CO.

# MULTI-DETECTOR ARRANGEMENTS FOR ON-LINE MEASUREMENTS OF γ-RAY AND NEUTRON MULTIPLICITIES*

A. KEREK, J. KIHLGREN, TH. LINDBLAD, C. POMAR†, J. SZTARKIER, W. WALUS+

*Research Institute of Physics, S-104 05 Stockholm, Sweden*

Ö. SKEPPSTEDT

*Chalmers University of Technology, S 402 20 Gothenburg, Sweden*

J. BIALKOWSKI, J. KOWNACKI, Z. SUJKOWSKI and A. ZGLIŃSKI

*Institute of Nuclear Research, 05-400 Swierk, Poland*

Received 15 August 1977

This paper describes multi-detector arrangements for measuring the number of quanta emitted in a cascade. Two set-ups are described, one with NaI(Tl) detectors and another with liquid scintillators. The latter system has the advantage of being able to separate between neutron and γ-ray events, which is of particular importance for reactions with a large number of neutrons emitted. The set-ups are used on-line the Stockholm cyclotron. Examples of experiments with 51 MeV α-particles and 118 MeV $^{12}$C-ions are presented.

## 1. Introduction

The structure of atomic nuclei at high angular momentum is an intriguing problem in today's nuclear physics and several interesting phenomena related to high-spin states have been uncovered during the last few years. Examples of such phenomena are "backbending"[1]) and rotation-alignment[2]).

Much of our knowledge of nuclear states with high spin-values has come from Coulomb excitation and (particle, $x$n) reaction experiments. However, although experiments may be chosen to impart angular momentum of 50–80 $\hbar$, only a few states with spin values in excess of 20 $\hbar$ have been established. This apparent gap between the angular momentum input in (HI, $x$n) reactions and the dissipation of angular momentum from the evaporation residues is, at present, not fully understood. In fact, little is known about the formation and decay of high spin states and their stability against fission (see e.g. refs. 3–5). The limiting angular momenta for compound nuclear reactions in the medium mass region are expected to be in the 40–70 $\hbar$ range and the angular momentum of the evaporation residues should not differ significantly from that of the compound system. Thus the main process of the dissipation of angular momentum is the electromagnetic radiation. The low multipolarity of this radiation (dipole and quadrupole) implies cascades consisting of a large number of γ-rays. Because of the relatively high level density several deexcitation channels are open for each evaporation residue. The resulting γ-ray spectrum observed with presently available detectors has therefore the form of a continuous distribution with superimposed discrete lines corresponding to the few final transitions of the cascades.

First attempts[6,7]) to measure the average number of γ-rays (the multiplicity) following (HI, $x$n) reactions were performed with a single γ-ray detector or with two detectors in coincidence. Recently, multi-detector arrangements have been used[8-11]) in order to yield information on the distribution of the multiplicity. Such set-ups normally involve a high-resolution Ge(Li) detector in coincidence with a set of several NaI(Tl) counters.

This paper describes two multi-detector arrangements designed for studies of γ-ray and neutron multiplicities. The first set-up is similar to those described in refs. 9, 10 and 11 and employs eight NaI (Tl) detectors in multi-coincidence mode with a single Ge(Li) spectrometer. The system allows for a reasonably high γ-ray detection efficiency but the geometry used does not allow to distinguish between neutron and γ-ray detection. Indeed, the

* Work supported in part by the Swedish Atomic Research Council (AFR).

† Permanent address: Departamento de Física Nuclear, Comisión Nacional de Energía Atómica, Buenos Aires, Argentina.

+ Permanent address: Department of Nuclear Physics, Jagiellonian University, 30-059 Cracow, Poland.

distance between the target and the NaI(Tl)-counters necessary for such a separation by means of time-of-flight method is of the order of 60 cm, which would imply a system with very big crystals for a practical experiment.

The second system is designed to distinguish between neutron and $\gamma$-ray events. For this reason, NE 213 liquid scintillators are employed together with pulse shape discriminating electronic circuits. An additional advantage of the liquid scintillator system may stem from the simultaneous determination of $\gamma$-ray and neutron multiplicity. The neutron multiplicity information can be used for identification of the exit channel in a heavy ion induced reaction. The system also allows to measure the distributions of neutron multiplicity in processes where this is not a sharp number (e.g. HI induced fission).

There are several problems involved with multiplicity measurements. Thus there are a great number of corrections to the measured coincidence spectra. In the subsequent section, the general idea about multiplicity experiments is outlined. In sect. 3 we describe the experimental arrangements and the last two sections describe the corrections and present examples of the multi-coincidence spectra for various (particle, $x$n) reaction experiments.

## 2. Experimental arrangements of the multi-detector system

The general layout of the multi-detector arrangement is shown in fig. 1. The detectors are housed in conical lead-shields which can be placed in 17 different positions in a semi-spherical holder made of aluminium and a plastic resin. Fig. 2 shows the cut through the horizontal plane of the set-up with a NaI(Tl)- and several liquid scintillation detectors. The minimum thickness of lead between two adjacent detectors is 4 cm in the NaI case and 2.5 cm when liquid scintillators are used. A Cd–Cu mantle surrounds the detectors in order to absorb the lead X-rays.

The NaI(Tl) detectors employed have a diameter of 5.1 cm and a height of 7.6 cm. When placed in the holder, the front of the detector is 15 cm from the target position. The NaI(Tl) crystals are coupled to EMI 9656 photomultiplier tubes with

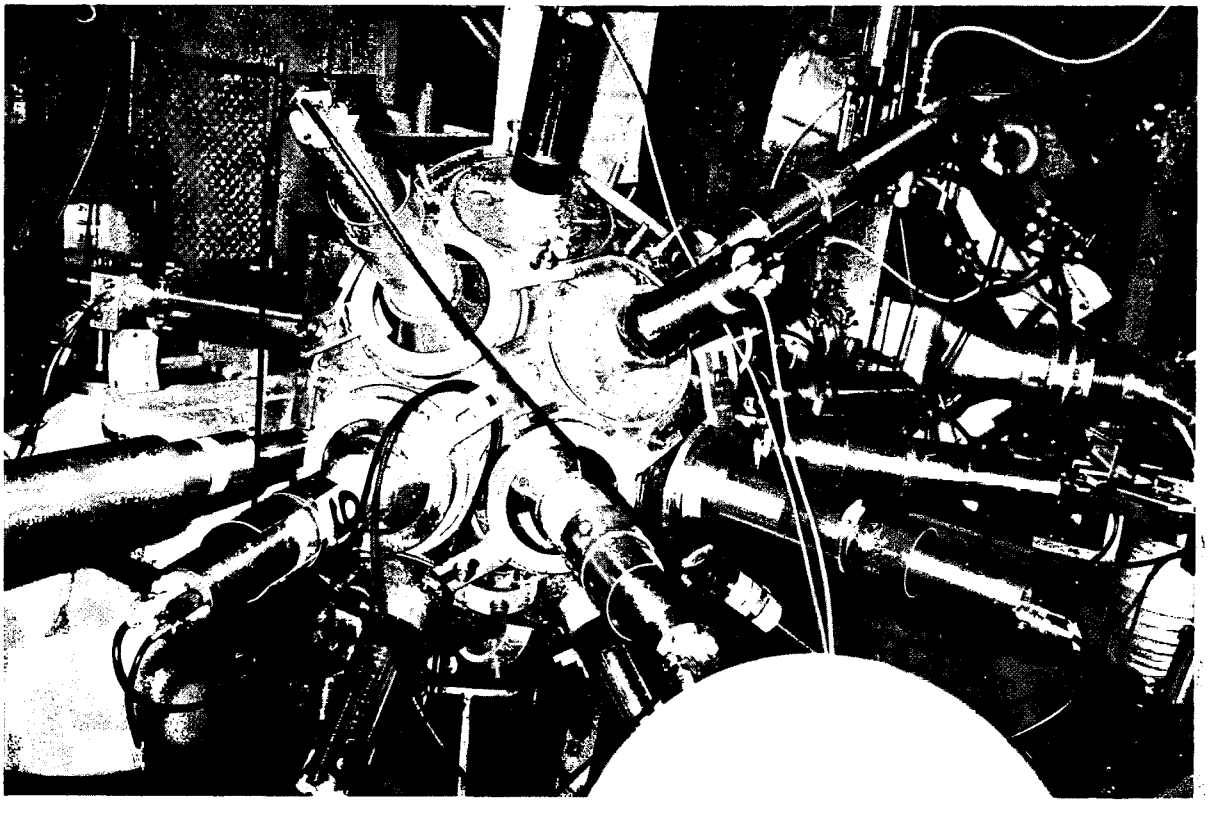

Fig. 1. Photography of the multi-detector arrangement.

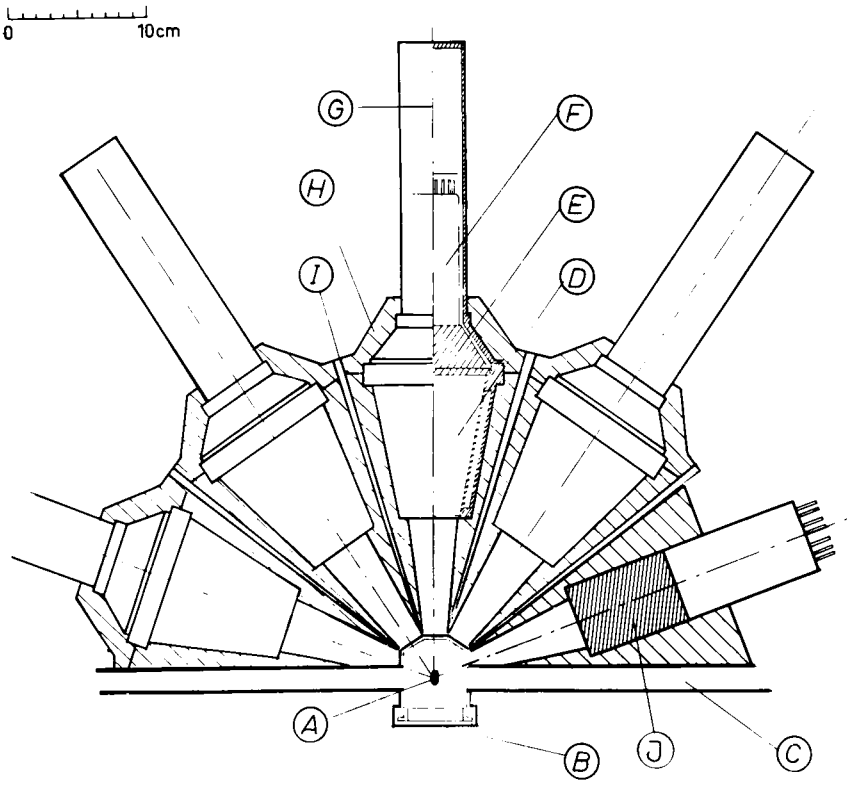


Fig. 2. A horizontal cut-through of the multi-detector arrangement. A total number of 17 detectors may be used, of which 5 are in the horizontal plane. Legend: A – target, B – target chamber window, C – beam tube, D – liquid scintillator, E – light guide, F – photomultiplier tube, G – PM-base with voltage stabilized dynode chain and preamplifier, H – lead shield, I – conical hole for the lead shield, J – NaI(Tl) detector. The liquid scintillation and NaI(Tl) detectors have their fronts 15 cm from the target.

partially voltage-stabilized dynode chains. A simple preamplifier with adjustable decay time constant is included in the base housing.

The liquid scintillator detectors are specially designed in cooperation with the manufacturer, Nuclear Enterprise Ltd, Edinburg. They are of the type where the expansion volume is in the surrounding walls. The photomultiplier tubes used with these scintillators are XP2020, again equipped with a voltage-stabilized dynode chain.

The Ge(Li) detector is placed in the horizontal plane opposite to the vertically positioned scintillator detector holder and can be moved over a large angle.

Fig. 3 shows the $\gamma$-ray efficiency curves for both types of detectors, determined with use of standard intensity calibrated IAEA radioactive sources and from multicoincidence measurements using radioactive isotopes with well-known decay schemes and hence known values of the multiplicity $M$.

The electronic arrangement following the outputs from the detectors is shown in fig. 4 for the liquid scintillator set-up. A CAMAC coincidence register (LRS 2340B) with $2\times 8$ inputs is used. One of the two blocks of inputs addresses the bits $2^0$–$2^7$ and the other one the bits $2^8$–$2^{15}$. Each of these blocks has an output signal proportional to the number of coincidences within the common gate. The resolving time of the coincidence register is typically set to 30 or 40 ns.

When using up to eight NaI(Tl) detectors, only one of the two eight-fold input blocks is needed. Then the anode pulses from the NaI(Tl) detector are fed to the LRS inputs via the preamplifiers. When the eight liquid scintillators are used in order to measure both the $\gamma$-ray and the neutron multiplicities both input blocks are required. The pulses from each liquid scintillator are fed to a fast constant fraction timing unit and a pulse-shape discriminating circuit[12]). The latter has two outputs, one giving a signal if a neutron is detected,

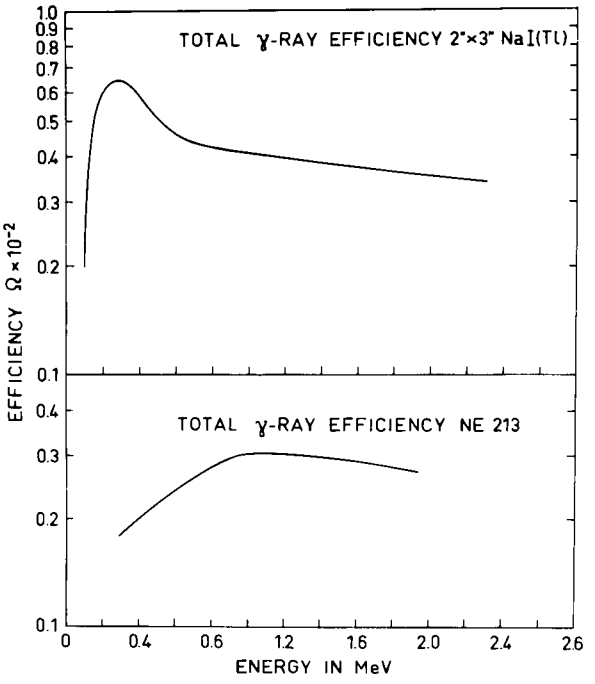


Fig. 3. Absolute $\gamma$-ray efficiency vs incident photon energy for the NaI(Tl) crystals and the liquid scintillators discussed in the text.

the other if a $\gamma$-ray event has occurred. Thus the two different signals are fed to the two separate input blocks of the coincidence register, while the gate event is the same, namely the pulse from the Ge(Li) detector.

Fig. 5 shows the separation of neutrons and $\gamma$-rays in one of the scintillation detectors during an actual run.

The information is stored on magnetic tape via the CAMAC system, the Ge(Li) energy as a 12-bit address, the multi-coincidence pattern as a 16 bit address. Thus by recording the actual pattern, information will be obtained on the angular distribution of the $\gamma$-rays and neutrons. A check that all detectors are working properly is also provided in this way.

In order to control the experiment and to be able to perform necessary dead-time corrections, the sum output signal from the coincidence register is used. The amplitude of this signal is proportional to the number of scintillation detectors (the fold) fired. By means of single channel analysers, signals can be generated corresponding to the various folds. These signals are fed into a multichan-

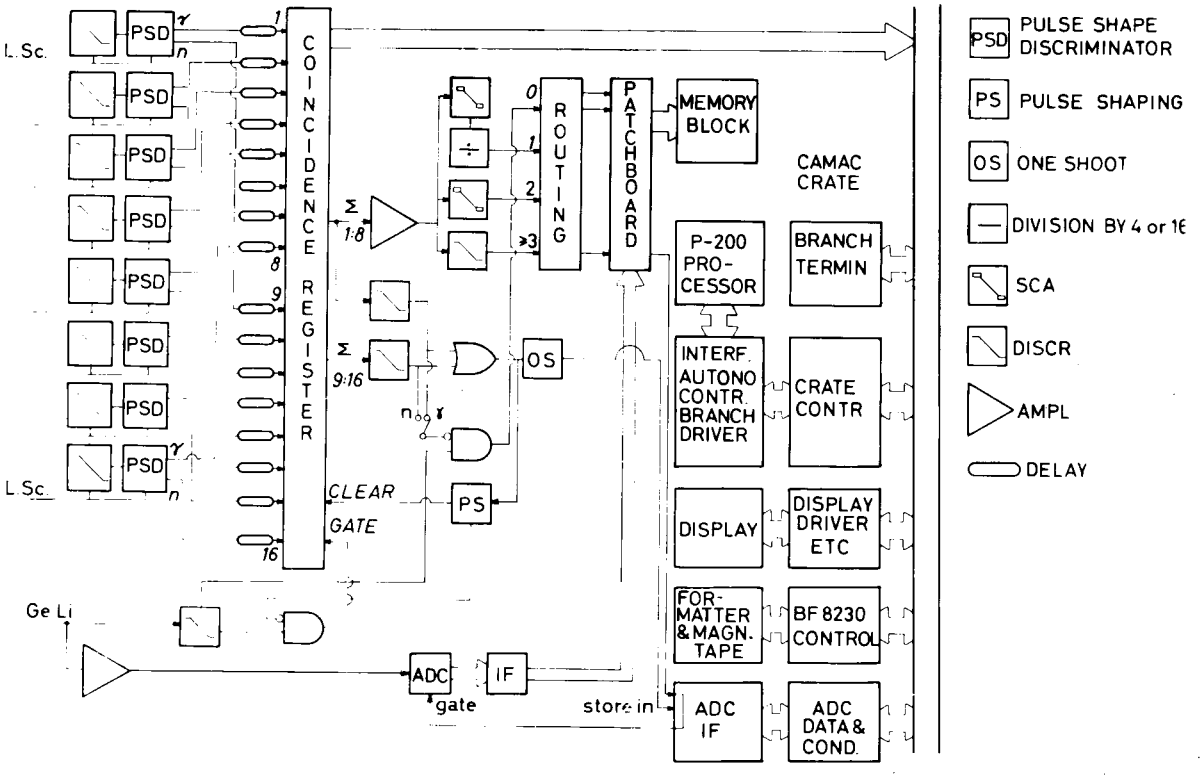


Fig. 4. The electronic data acquisition system used together with eight liquid scintillators for $\gamma$-ray and neutron multiplicity measurements. The n–$\gamma$ switch determines which of the two multiplicity spectra will be stored in the memory block.

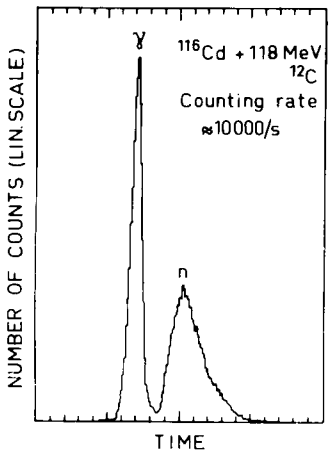


Fig. 5. Spectrum showing the separation between neutrons and $\gamma$-rays using liquid scintillation detector and pulse-shape discriminator. The threshold of the pulse-shape discriminator was set at about 700 keV neutron energy.

nel analyser via a routing system and the energy signal from the Ge(Li) detector is directly analysed with respect to the fold. Fig. 4 shows such an arrangement for recording the 0, 1, 2 and 3-fold coincidence spectra (0-fold is corresponding to events when none of the scintillation detectors were fired). Since the 1-fold coincidences are very frequent, arrangements are made in order to divide the number of these events by 4 or 16 before storing the data on magnetic tape and in the memory block. In order to make a full analysis of the data it is necessary to use the singles or the 0-fold spectra. These spectra are not recorded on magnetic tape but stored in a memory block.

The counting rates of the various folds are measured during the run using scalers. Since the 1- and 2-fold coincidences are recorded both on magnetic tape and in the memory block, it is possible to correct for the dead time of the CAMAC system and the magnetic tape station.

### 3. Multi-coincidence probabilities and moments of multiplicity distributions

For simplicity we shall start by considering a case of $M+1$ $\gamma$-rays in a cascade. If the photons are detected in a single Ge(Li) crystal, with the counting rate $Q^{\mathrm{Ge}}$, and this detector provides a "gate event" for coincidences among $N$ identical scintillation counters, the counting rate for $p$-fold coincidences may be written:

$$Q_{Np} = Q^{\mathrm{Ge}}\, P_{Np}[M, \Omega_i(E), \alpha(E), W(\theta, \phi)], \qquad (1)$$

where $P_{Np}$ is the overall probability that out of $N$ detectors $p$ will be in coincidence within the gate. $\Omega_i(E)$ is the $\gamma$-ray efficiency for the $i$th detector, $\alpha(E)$ are the conversion coefficients for the $\gamma$-rays detected and $W(\theta, \phi)$ is the angular correlation function. In addition to the relationship (1) $Q_{Np}$ depends on the probability that one detector may record more than one quantum. This summing effect for the scintillation detectors is taken into account in the following formula valid for the assumptions that $\Omega_i(E) = \Omega = \text{constant}$ and that the internal conversion and angular dependences may be neglected:

$$P_{Np} = \binom{N}{p} \sum_{k=0}^{p} (-1)^{k-p} \binom{p}{k} [1 - (N-k)\,\Omega]^M . \qquad (2)$$

This, in fact, is the sum of the probabilities that nothing was detected in any combination of $(N-k)$ detectors while $k$ varies from 0 to $p$. Quantitatively, this is equivalent to the expressions derived in ref. 9.

In the cases when $M, N \ll \Omega^{-1}$ eq. (2) may be approximated by a more transparent expression

$$P_{Np} \simeq \binom{N}{p} \mathrm{e}^{-N\Omega M} (\mathrm{e}^{M\Omega} - 1)^p , \qquad (3)$$

which is useful for a quick comparison of various $P_{Np}$ and their dependence on the entering param-

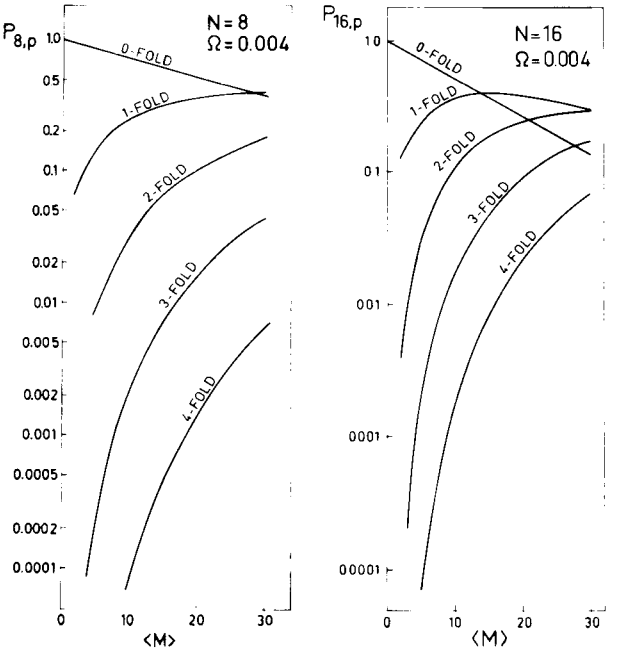


Fig. 6. The probability $P_{Np}$ of recording a $p$-fold event when $M+1$ coincident $\gamma$-rays are emitted. 8 and 16 detectors are used, each with an average total efficiency of 0.004.

eters. In particular, the ratio of two consecutive fold probabilities is equal to

$$\frac{P_{Np}}{P_{N,p-1}} = \frac{N-p+1}{p}(e^{M\Omega}-1). \tag{3a}$$

The coincidence probabilities of eq. (2) are plotted in fig. 6 as functions of the multiplicity for $N=8$ and $N=16$ detectors, each with the efficiency $\Omega=0.004$. It can be seen that the probability of higher fold coincidences strongly depends on both $M$ and $N$ (see also appendix).

The experimental values pertinent to eq. (2) are the ratios

$$\frac{I_p}{I_{tot}} = P_{Np}^{exp} = \sum_{M=0}^{\infty} f(M)\, P_{Np}, \tag{4}$$

where $I_p$ is the number of counts in a peak in the $p$-fold spectrum, $I_{tot}$ is the number of counts in this peak in the corresponding singles spectrum and $f(M)$ is the multiplicity distribution. In order to extract the average multiplicity $\langle M\rangle$ and information on the multiplicity distribution various methods may be applied.

In the following we use some of the results from the analysis in ref. 10, in which several extensions and generalizations have been introduced of the treatment of the subject in ref. 9. Thus one can introduce a quantity $R_p$, representing the probability for observing a $p$-fold coincidence event if only $p$ detectors were present, i.e.

$$R_p = P_{pp} = \sum_{m=0}^{p} (-1)^m \binom{p}{m} (1-m\Omega)^M. \tag{5}$$

The experimentally determined ratios (4) are related to the new quantities $R_p$ by

$$R_p = \binom{N}{p}^{-1} \sum_{k=p}^{N} \binom{k}{p} P_{Nk}^{exp}. \tag{6}$$

Expanding eq. (5) in powers of $\Omega$ and setting $p_{max} \leq N$ we get

$$R_p = \sum_{m=1}^{m_{max}} Y_{pm} X_m, \tag{7}$$

where

$$Y_{pm} = \frac{1}{m!} \sum_{k=1}^{p} (-1)^{k+m} \binom{p}{k} k^m, \tag{8}$$

and

$$X_m = \langle M(M-1)(M-2) \ldots (M-m+1)\rangle\, \Omega^m. \tag{9}$$

By solving the set of eq. (7) for $X_m$, one gets

$$X_m = \frac{1}{I_{tot}} \sum_{k=m}^{p_{max}} \alpha_{mk} I_k, \tag{10}$$

where $\alpha_{mk}$ can be calculated from the recurrence relationship

$$\sum_{j=m}^{k} Y_{mj}\alpha_{jk} = \binom{k}{m} \Big/ \binom{N}{m}. \tag{10a}$$

From the $X_m$ values, we may now try to extract information on the multiplicity distribution. Thus by introducing

$$\mu = \langle M\rangle = X_1 \Omega^{-1}, \tag{11}$$

and the central moments

$$\mu_p = \langle (M - \langle M\rangle)^p\rangle, \tag{12}$$

we find that

$$\mu_1 = 0, \tag{13a}$$

$$\mu_2 = X_2\Omega^{-2} - \mu(\mu-1), \tag{13b}$$

$$\mu_3 = X_3\Omega^{-3} - 3\mu_2(\mu-1) - \mu(\mu-1)(\mu-2), \tag{13c}$$

etc.,

which gives us the variance and skewness as

$$\sigma = (\mu_2)^{\frac{1}{2}}, \tag{14a}$$

and

$$s = \mu_3/\sigma_3, \tag{14b}$$

respectively.

It should be noted that the various coincidence folds are not completely independent. The truncation made by setting the highest fold observed $p_{max} = N$, is a fair approximation provided that $\Omega$ is small*).

The statistical accuracies obtainable under normal experimental conditions put severe restrictions on the determination of higher moments of the multiplicity distribution. In fact, a detailed analysis of assumed symmetric and asymmetric triangular shapes of the distribution (cf. appendix) shows that already the third moment (the skewness) is extremely difficult to determine within any significant level of confidence.

## 4. Corrections to the multiplicities

There are several corrections to the multiplicities and the higher moments derived from the method discussed above. In the following subsections several of these corrections are discussed in some detail.

### 4.1. Corrections due to neutrons detected in the NaI(Tl) crystal

Since it is not possible to distinguish between neutrons and $\gamma$-rays with the NaI(Tl) detector ar-

* This problem, as well as other methods of analysing the multiplicity data are discussed in e.g. refs. 15–17.

rangement, a correction for "neutron events" has to be included. This correction is most transparent if we consider the multiplicity obtained from the approximate expression given by eq. (3a), which may be rewritten as

$$\frac{P_{N,p}}{P_{N,p-1}} = \frac{N-p+1}{p}\,(e^{M\Omega}\,\mathrm{e}^{x\Omega_n}-1), \tag{15}$$

where $x$ is the number of evaporated neutrons and $\Omega_n$ is the average neutron efficiency of the NaI(Tl) detector. Thus the corrected multiplicity is obtained by a simple subtraction, i.e.

$$\langle M\rangle \rightarrow \langle M\rangle - x\Omega_n/\Omega\,. \tag{16}$$

The $\Omega_n/\Omega$ ratio may be determined in a separate experiment with, e.g., the time-of-flight technique. Care should be taken that the effects of neutron scattering from the surroundings into the detectors are similar in both the multiplicity and the time-of-flight measurements. The ratio depends on the reaction studied and should be determined separately for each exit channel, especially in cases where preequilibration effects are not negligible. In the experimental conditions of this work the $\Omega_n/\Omega$ ratio was of the order of 0.10.

### 4.2. Corrections due to the use of an average detector efficiency

The average total $\gamma$-ray efficiency $\Omega$ for the scintillators can be obtained from the absolute efficiency curve measured with calibrated sources (cf. fig. 3) if the true spectrum of emitted quanta is known. The latter may be obtained from e.g., unfolding the energy spectrum measured with a high resolution detector [Ge(Li), preferrably surrounded by a Compton-suppression detector]. In most cases a sufficient approximation, however, is to unfold the amplitude spectra from the scintillators used. In order to do this the tabulated response functions may be used in the case of the NaI(Tl) detectors, and a simple differentiation of the amplitude distribution in the case of the liquid scintillators (corrections for the second chance Compton interaction within the scintillator volume can be included in a straightforward fashion).

The use of an average $\gamma$-ray efficiency introduces an error in the calculations discussed in section 3. As far as the resolved lines in the measured spectra are concerned, this effect may be corrected for, provided that the decay scheme is known. In essence, the contribution from resolvable transitions to the measured probability for detecting a multi-coincidence event can be accounted for explicitly by plugging the actual $\gamma$-ray efficiencies, branchings and side-feeding fractions into the formulae. Exact formulae for this procedure are given in ref. 10.

For a case of a straight cascade (i.e. without branchings) of $s$ $\gamma$-rays following the gating transition, a simple correction for the known efficiencies $\Omega_k$ can be introduced. The average efficiency $\Omega$ should be replaced by

$$\Omega \rightarrow \Omega \Big/ \left[1 + \frac{\sum_{k=1}^{s} (\Omega - \Omega_k)}{\langle M^{\mathrm{uncorr}}\rangle\,\Omega}\right], \tag{17}$$

where $\langle M^{\mathrm{uncorr}}\rangle$ is the uncorrected multiplicity value deduced from eq. (11). The average multiplicity value $\langle M_{\mathrm{in}}\rangle$ for the transitions preceeding the gating one can thus be expressed as

$$\langle M_{\mathrm{in}}\rangle = \langle M^{\mathrm{uncorr}}\rangle - \sum_{k=1}^{s} \Omega_k \Big/ \Omega\,. \tag{18}$$

Note that neither here, nor in the previous discussions, we have considered the transition detected in the Ge(Li) spectrometer. The total multiplicity in this notation is always $\langle M\rangle + 1$.

### 4.3. Corrections due to internal conversion

If the average conversion coefficient $\alpha$ is known, we may include a correction which is due to the fact that those transitions taking place by means of internal conversion are not observed. This correction is included by means of the substitution

$$\Omega \rightarrow \Omega/(1+\alpha), \tag{19}$$

for the average efficiency. Clearly, certain assumptions on the multipolarity have to be made in order to obtain $\alpha$.

### 4.4. Corrections due to angular correlations of the $\gamma$-rays

A detailed description of the angular correlation effects can be found in ref. 13. It is also pointed out there that the corrections depend strongly on the geometry and by suitable placement of the detectors the corrections can be kept small. In this case, the following approximate correction formulae, given in ref. 10 can be used.

Thus the peak areas of the 1-fold spectrum should be divided with

$$\langle W_1\rangle = N^{-1}\,[W_1(\theta_{\mathrm{Ge}}, \theta_1) + W_1(\theta_{\mathrm{Ge}}, \theta_2) + \ldots + W_1(\theta_{\mathrm{Ge}}, \theta_N)], \tag{20}$$

where $\theta_{Ge}$ is the angle of the Ge(Li) spectrometer and $\theta_i$ the eight angles of the NaI(Tl) detectors. The corrections to the higher-fold spectra, are

$$\langle W_p \rangle = \langle W_1 \rangle [1 - (p-1)\tfrac{1}{2}(1 - \langle W_1 \rangle)], \quad (21)$$

or simply $\langle W_p \rangle \approx \langle W_1 \rangle$ which only gives an error of 1% or 2% compared with eq. (21).

### 4.5. Correction due to coincidence summing and cross-scattering

According to ref. 9, summing in the Ge(Li) detector may be taken into account by multiplying the scintillation detector efficiency $\Omega$ by $(1-\Omega_0)^{-1}$, where $\Omega_0$ is the total average efficiency of the Ge(Li) detector.

In order to estimate the number of false coincidences due to cross-talk between the NaJ(Tl) detectors, a coincidence measurement was performed with all but one of the detectors shielded from the target by 12 cm thick lead cones.

The true 1-fold coincidences then come from the unscreened detector, while the 2-fold events are due to Compton scattering from the open crystal detected in one of the other detectors. After correction for the transmission of gamma rays through the lead shields, the cross-talk was calculated to increase the 2-fold coincidence rate by $\leq 1.5\%$.

### 4.6. Corrections due to coincidences between $\gamma$-rays following two reactions

Another important source of false coincidences is due to $\gamma$-rays following two reactions, within the same beam burst or within the coincidence resolving time in the case of a continuous beam. The average $\gamma$-ray multiplicity of such an event is then doubled. This actually limits the possibility of a meaningful determination of the higher-fold ratios. The importance of this effect was first pointed out by Ockels and Greeuw, KVI, Groningen, and can be illustrated by the following example.

Assume that the multiplicity is 15 and that the ratio of double-to-single events is 0.01. This gives, if 8 detectors with $\Omega = 0.004$ are used, an increase by 1.1% for the 1-fold, 2.6% for the 2-fold, 5.8% for the 3-fold, 14,2% for the 4-fold, and 32% for the 5-fold probability.

The number of "double reactions" was estimated by measuring the time spectrum taken between two detectors (cf. fig. 7). The first peak (A) is mainly due to the true coincidence events. The second peak (C), one beam burst later, is a false one due to signals from $\gamma$-rays (or neutrons) coming from two different nuclei produced one beam burst apart in time. The ratio C/A is approximate-

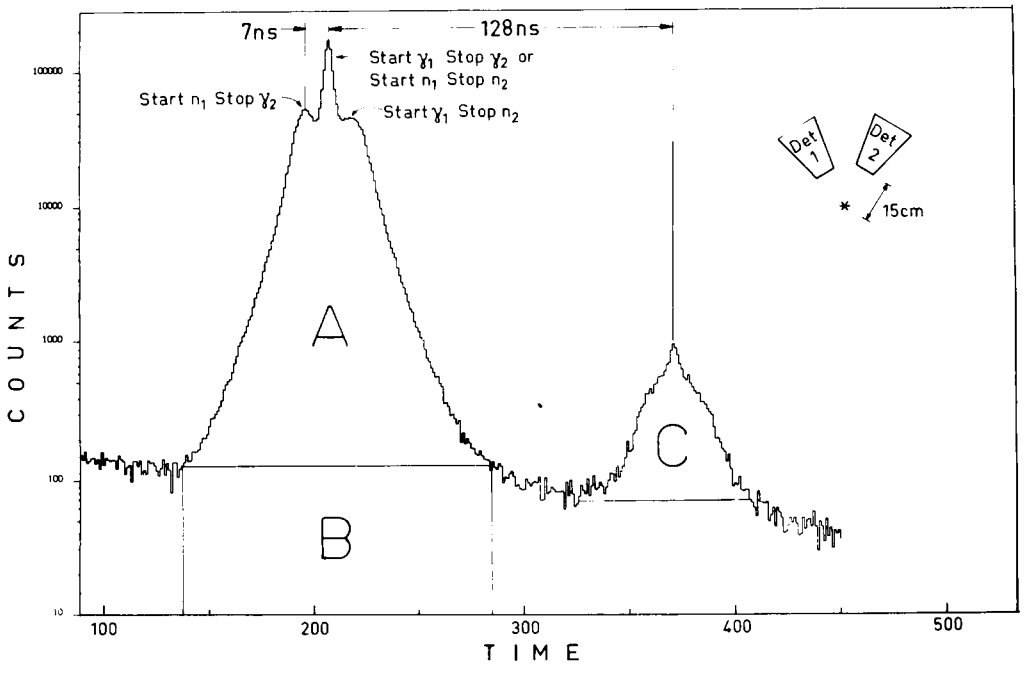


Fig. 7. Example of time spectrum between two detectors. Events associated with area A are mainly due to true and B to random coincidences. The second peak (C) has its origin in events when the start and the stop signals are generated by $\gamma$-rays (or neutrons) from two different nuclei produced one beam burst apart in time. During the experiments the ratio A/C was kept $>150$.

ly equal to the reaction probability per beam burst times the multiplicity. In order to have the double-to-single event ratio equal approximately to 0.001, the ratio A/C should be kept above $\sim 100$. From the time spectrum shown in fig. 7 it is also possible to estimate the number of random coincidences due to radioactivity (B).

## 5. Examples of measurements

Experiments have been performed with eight NaI(Tl) detectors or eight liquid scintillation detectors. The latter were used in conjunction with experiments where targets were bombarded with 118 MeV $^{12}C$ and up to eight neutrons were evaporated from the compound nucleus, while the NaI(Tl) detectors were used for ($\alpha$, 3n) and ($\alpha$, 4n) experiments.

### 5.1. Experiment using eight NaI(Tl) detectors

A self-supporting metallic target of $^{166}Er$ (enrichment >96%), was prepared to a thickness of $\approx 3$ mg/cm$^2$. The target was bombarded with 51 MeV $\alpha$-particles, i.e. the optimum energy for producing the $^{166}Yb$ final nucleus. The Ge(Li) detector used in this and in subsequent experiments has at 1.33 MeV an efficiency of 11%, a resolution of 2.0 keV (fwhm), the peak height to Compton edge height ratio of 37:1 and peak to total ratio of $\sim 0.07$.

During the experiment, $\approx 33$ million events were recorded on magnetic tape. These tapes were subsequently analysed and the various spectra corresponding to $p = 1, 2, 3 \ldots$ were obtained (fig. 8). The results of the analysis for the first two moments of the multiplicity distribution are summarized in figs. 9 and 10. The total multiplicity is found to increase with increasing spin value, while the width of the distribution is constant ($\sigma = 4$). For detailed information how to extract the side-feeding multiplicity, we refer to ref. 10.

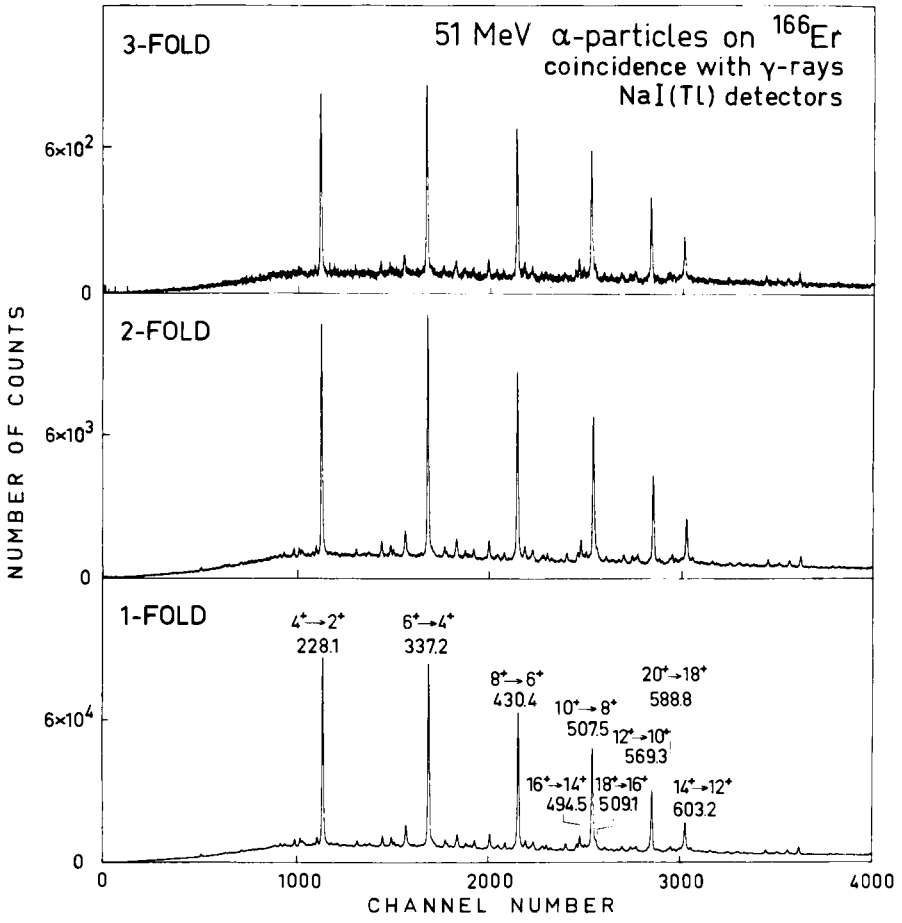


Fig. 8. Examples of coincidence spectra from the $^{166}Er(\alpha, 4n)$ reaction at $E_\alpha = 51$ MeV.

### 5.2. Experiment using eight liquid scintillator detectors

A self-supporting $^{176}$Yb target (enrichment >96%) was bombarded with 118 MeV $^{12}$C ions. Neutron and gamma ray patterns from the multi-coincidence arrangement were recorded on magnetic tape. The singles spectrum of the gamma rays and spectra of the first folds were recorded simultaneously in a multi-channel analyser. The time distribution was monitored separately on a PDP-9 computer.

The results for the $\gamma$-ray multiplicity summarized in fig. 11 show that the average gamma-ray multiplicity $\langle M \rangle$ increases from 15.5 for the $2^+ \rightarrow 0^+$ transition to 19 for the $14^+ \rightarrow 12^+$ transition, while the width $\sigma$ is constant and around 6 units.

### 5.3. Neutron multiplicities

The neutron coincidence spectra obtained during bombardment of $^{176}$Yb with 118 MeV $^{12}$C are displayed in fig. 12. An analysis of the strong lines, which all correspond to transitions from the $^{176}$Yb($^{12}$C, 8n)$^{180}$Os reaction is shown in fig. 13a.

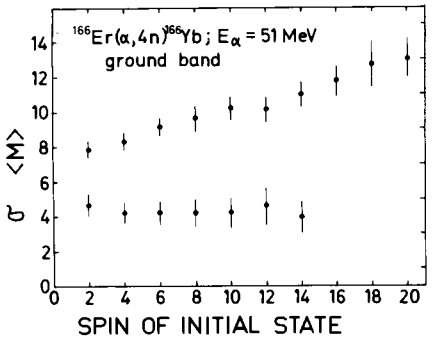


Fig. 9. Experimental values of the multiplicity $\langle M \rangle$ and width $\sigma$ of the multiplicity distribution as function of spin $I$ for the $^{166}$Er($\alpha$, 4n)$^{166}$Yb reaction at 51 MeV.

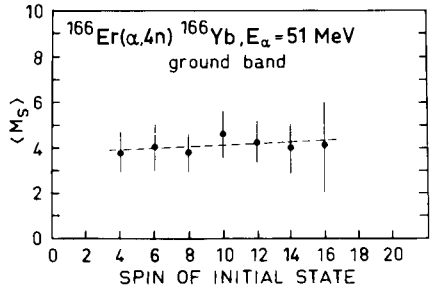


Fig. 10. Multiplicities of side feeding of the ground band as a function of spin $I$ for the $^{166}$Er($\alpha$, 4n)$^{166}$Yb reaction at 51 MeV.

The quantity $\langle M\Omega \rangle$, where $M$ is the neutron multiplicity and $\Omega$ is the liquid scintillator efficiency for neutron detection, remains constant within the errors for all the transitions. The same analysis was made for the $^{160}$Gd($^{12}$C, 8n)$^{164}$Yb and $^{160}$Gd($^{12}$C, 6n)$^{166}$Yb reactions at 118 MeV incident energy and the ratios of corresponding transitions from the two reactions are shown in fig. 13b. The ratios are close to $8/6 = 1.3$ as expected for reactions when 8 and 6 neutrons are evaporated respectively. The set-up might thus be used as a tool for reaction identification. In particular, the reaction channels of the type (HI, $\alpha$xn) and (HI, 2p($x$+2)n) could be distinguished without detecting the $\alpha$-particle.

Since five of the eight detectors are in one plane it is possible to directly obtain the angular distributions of the neutrons (fig. 14). It should however be born in mind that no correction for the change of detector efficiency with neutron energy has been applied while significant variations of the neutron energy spectra with the laboratory angle may be expected.

The multi-detector systems of the types described may also be applied as valuable spectroscopic tools, e.g. as multiplicity filters accentuating detection of transitions between very high spin states or locating high spin isomeric states etc. The description of such applications, which is out-

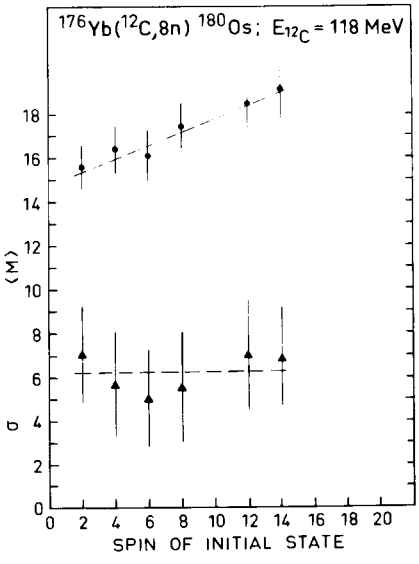


Fig. 11. Measured values of the multiplicity $\langle M \rangle$ and width $\sigma$ of the multiplicity distributions as a function of spin $I$ of initial states for the $^{176}$Yb($^{12}$C, 8n)$^{180}$Os reaction at 118 MeV.

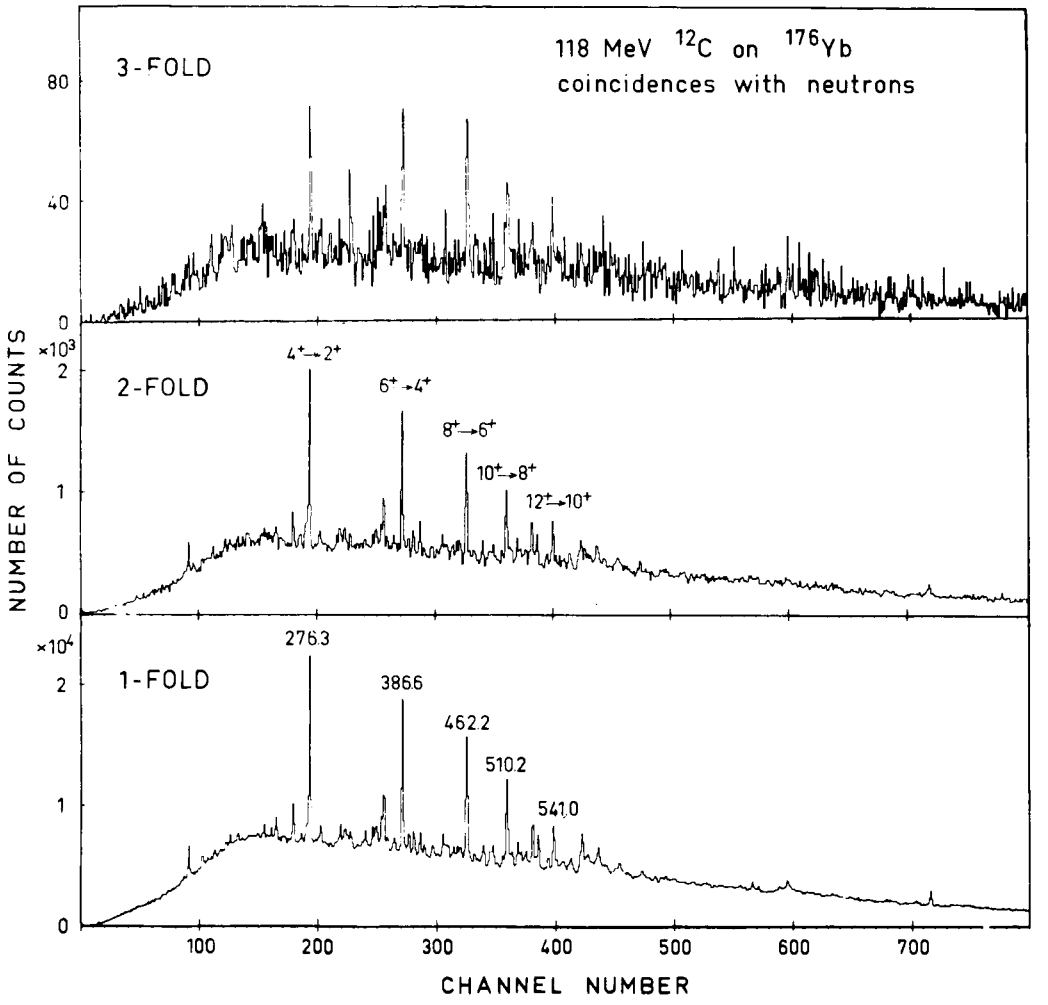


Fig. 12. Gamma-ray spectra, in multiple coincidence with neutrons detected with liquid scintillators, resulting from the bombardment of $^{176}$Yb with 118 MeV $^{12}$C.

TABLE 1

Calculated contributions $S_k$ to the final error $\delta\mu_3$ from various coincidence folds for $\Omega = 0.004$, $I_{tot} = 10^5$. $\delta\mu_3 = (\sum_k S_k)^{\frac{1}{2}}$

| $\langle M \rangle$ | $N$ | $S_1$ | $S_2$ | $S_3$ | $S_4$ | $S_5$ | $S_6$ | $S_7$ | $\sum_{k=1}^{7} S_k$ |
|---|---|---|---|---|---|---|---|---|---|
| 5 | 8 | 4 | 50 | 114 | 90 | 12 | 1 | 0 | 271 |
| | 16 | 1.6 | 7.2 | 3.0 | 10.0 | 3.3 | 0.4 | 0.0 | 25.5 |
| | 24 | 0.9 | 1.8 | 0.1 | 2.2 | 1.4 | 0.3 | 0.0 | 6.7 |
| 9 | 8 | 75 | 480 | 264 | 1 027 | 450 | 75 | 6 | 4 377 |
| | 16 | 28 | 38 | 1 | 49 | 72 | 32 | 7 | 227 |
| | 24 | 14 | 3 | 4 | 3 | 17 | 15 | 6 | 62 |
| 15 | 8 | 875 | 2 202 | 10 | 4 435 | 5 187 | 2 014 | 395 | 15 118 |
| | 16 | 267 | 31 | 120 | 15 | 316 | 423 | 239 | 1 411 |
| | 24 | 110 | 11 | 21 | 10 | 13 | 82 | 106 | 353 |

side the scope of this paper, will be treated separately.

Results obtained with the systems described in this paper will be published elsewhere[14]).

The experimental set-ups used are parts of a larger project carried out in collaboration with the KVI laboratory, Groningen. The experimental facilities of the KVI laboratory will be presented in a separate paper. The present authors benefited greatly from experience gained during experiments in Groningen and from discussions with especially Drs. W. J. Ockels and M. J. A. de Voigt, as well as with the participants of the multiplicity workshop in Swierk, June 13-16, 1977.

## Appendix

*Analysis of the accuracies required to determine higher moments of the gamma ray multiplicity distribution*

Assume that we want to distinguish between two triangular multiplicity distributions, an asymmetric and a symmetric one as shown in fig. 15, with the same mean value and variance. The skewnesses of these distributions are $-0.566$ and 0, respectively, and the difference of the third moments $\Delta\mu_3 = |\mu_3^{\text{sym}} - \mu_3^{\text{asym}}| = 0.566\,\sigma^3$. What is the experimental accuracy required for the multifold spectra?

It follows from eq. (13c) that the experimental error in $\mu_3$ is given by the expression

$$(\delta\mu_3)^2 = \mu_3^2 \left|\frac{\delta I_{\text{tot}}}{I_{\text{tot}}}\right|^2 + \mu_3^2 \left|\frac{\delta\Omega}{\Omega}\right|^2 + \frac{1}{\Omega^2} \sum_{k=1}^{P\max} a_{Nk}^2 \langle P_{Nk}\rangle^2 \left|\frac{\delta I_k}{I_k}\right|^2, \tag{22}$$

where

$$a_{Nk} = [3\langle M\rangle(\langle M\rangle - 1) + 1 - 3\sigma^2]\,\alpha_{1k} - \frac{3(\langle M\rangle - 1)}{\Omega}\,\alpha_{2k} + \frac{1}{\Omega^2}\,\alpha_{3k}. \tag{23}$$

In an idealized case when the relative errors $\delta I_{\text{tot}}/I_{\text{tot}} = 0$, $\delta\Omega/\Omega = 0$, and $\delta I_k = \sqrt{I_k}$, expression (22) can be rewritten as

$$(\delta\mu_3)^2 = \frac{1}{I_{\text{tot}}\Omega^2} \sum_{k=1}^{P\max} a_{Nk}^2 \langle P_{Nk}\rangle. \tag{24}$$

Two sets of calculations were performed, with $\langle M\rangle = 5$, $\sigma^2 = 3$ and $\langle M\rangle = 15$, $\sigma^2 = 28$, for various numbers of detectors, $N$, and average efficiencies,

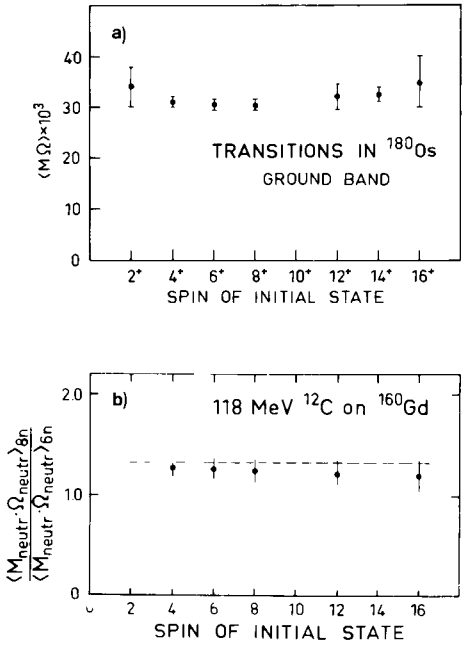


Fig. 13. (a) Measured values of $\langle M\Omega\rangle$ as a function of spin of initial state for the $^{176}$Yb($^{12}$C, 8n)$^{180}$Os reaction at 118 MeV. $M$ is the neutron multiplicity and $\Omega$ is the liquid scintillator efficiency for neutron detection. (b) Ratio $\langle M\rangle_{8n}/\langle M\Omega\rangle_{6n}$ for corresponding transitions from the two reactions $^{160}$Gd($^{12}$C, 8n)$^{164}$Yb and $^{160}$Gd($^{12}$C, 6n)$^{166}$Yb at 118 MeV incident energy. The dashed line indicates the theoretical value 8/6 = 1.33.

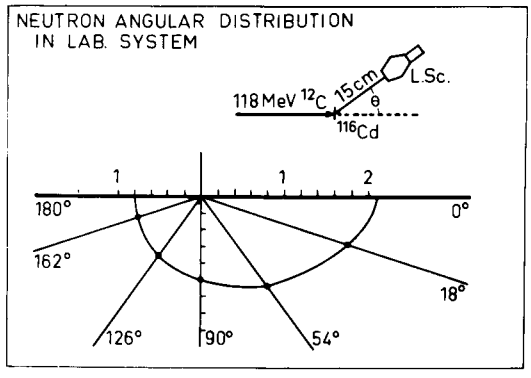


Fig. 14. Angular distribution of the neutrons emitted in the $^{116}$Cd($^{12}$C, $x$n) reactions at 118 MeV.

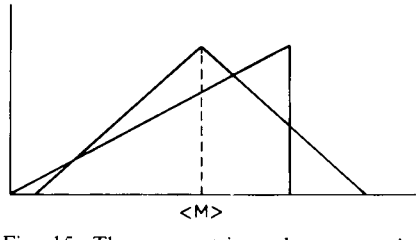


Fig. 15. The symmetric and asymmetric triangular distributions with the same mean value $\langle M\rangle$ and variance $\sigma^2$. The skewnesses of these distributions are 0 and $-0.566$, respectively.

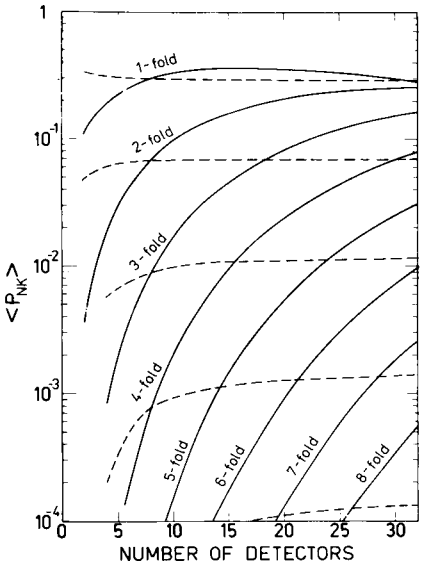


Fig. 16. Dependence of $\langle P_{Nk} \rangle$ on the detector number $N$ and efficiency $\Omega$ for the triangular distribution with $\langle M \rangle = 15$, $\sigma^2 = 28$. The solid lines correspond to $\Omega = 0.004$, the broken lines correspond to a constant product $N = 0.032$.

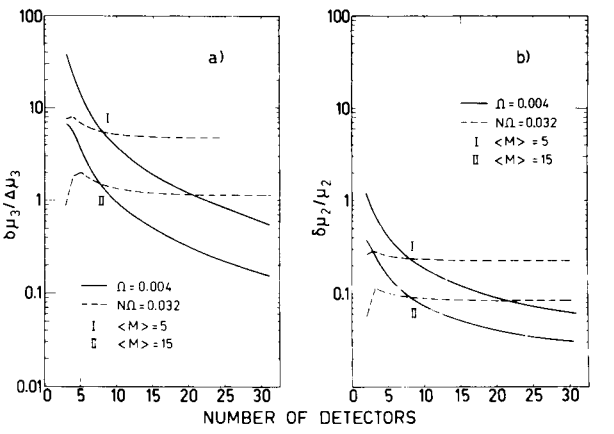


Fig. 17. Calculated errors in $\mu_3$ (a) and $\mu_2$ (b), expected in the idealized case for two triangular multiplicity distributions with $\langle M \rangle = 5$, $\sigma^2 = 3$ and $\langle M \rangle = 15$, $\sigma^2 = 28$. The assumed number of counts is $I_{tot} = 10^5$. The seeming superiority of the lowest $N$ is not real and it is caused by setting $p_{max} \ll \langle M \rangle$ in eq. (7).

$\Omega$. Fig. 16 shows the dependence of $\langle P_{Nk} \rangle$ on the detector number and efficiency for the triangular distribution with $\langle M \rangle = 15$. Fig. 17a shows the ratio $\delta\mu_3/\Delta\mu_3$ plotted vs $N$, for a typical number of counts under the peak in the total (singles) spectrum $I_{tot} = 10^5$. In order to distinguish between the symmetric and the asymmetric shape of the distribution, this ratio should be kept well below 1. Theoretically, this can be achieved, e.g., by increasing the detector number. In practice, however, the gain is slow because the very weak higher folds (6-fold, 7-fold, ...) contribute then with increasing weights to the estimated error. This is illustrated in table 1 where relative contributions to the final error from various coincidence folds are calculated for several values of $N$ and $\langle M \rangle$. The ratio depends also on the expected multiplicity value.

In the idealized sample case of fig. 17a with $\langle M \rangle = 15$, a meaningful determination of the third moment is attained for $N \gtrsim 20$, $\Omega = 0.004$. It should be noted that the figures of merit for skewness for $N\Omega = \text{const.}$ are nearly independent of $N$ for the $N$ value sufficiently large. Thus an alternative though usually less practical way of improving the conditions for determining $\mu_3$ is to increase the detector efficiencies.

In general it may be concluded that except for very large $\langle M \rangle$ values a practical determination of $\mu_3$ requires specially designed, very efficient multidetector arrangements. With the set-ups presently described the statistics necessary for such a determination would be almost prohibitively large.

Fig. 17b shows results of a similar analysis for the relative error of the second moment. Reasonable small errors are here easily attainable even with rather low detector number and moderate statistics.

## References


1) A. Johnson, H. Ryde and J. Starkier, Phys. Lett. **34B** (1971) 605.
2) F. S. Stephens and R. S. Simon, Nucl. Phys. **A183** (1972) 257; F. S. Stephens, R. M. Diamond, J. R. Leigh, T. Kammuri and K. Nakai, Phys. Rev. Lett. **29** (1972) 438.
3) M. Lefort, Suppl. J. Physique **37** (1976) C5-57.
4) S. Cohen, F. Plasil and W. J. Swiatecki, Ann. Phys. **82** (1974) 557.
5) A. Bohr and B. R. Mottelson, Physica Scripta **10A** (1974) 13.
6) J. F. Mollenauer, Phys. Rev. **127** (1962) 867.
7) E. der Mateosian, O. C. Kistner and A. W. Sunyar, Phys. Rev. Lett. **33** (1974) 596.
8) P. O. Tjøm, F. S. Stephens, R. M. Diamond, J. de Boer and W. E. Meyerhof, Phys. Rev. Lett. **33** (1974) 593.
9) G. B. Hagemann, R. Broda, B. Herskind, M. Ishihara, S. Ogaza and H. Ryde, Nucl. Phys. **A245** (1975) 166.
10) D. G. Sarantites, J. H. Becker, M. L. Halbert, D. C. Hensley, R. A. Dayras, E. Eichler, N. R. Johnson and S. A. Gronemeyer, Phys. Rev. **14C** (1976) 2138; L. Westerberg, D. G. Sarantites, R. Lorett, J. T. Hood, J. Barker, C. M.

Currie and N. Mullani (St. Louis, USA), to be published.
[11]) W. J. Ockels, M. J. A. de Voigt, Z. Sujkowski, J. van Klinken, S. J. Feenstra, G. Greeuw and A. Kerek, KVI Annual Report, Groningen (1976) p. 70.
[12]) J. Bialkowski and U. Szczepankowski, to be published.
[13]) O. Andersen, R. Bincer, G. B. Hagemann, M. L. B. Halbert, B. Herskind, M. Neiman and H. Oeschler, Risø preprint (1976).
[14]) Stockholm–Swierk–Groningen collaboration. Contributions to Int. Symp. on *High spin states,* Dresden (1977) and to Int. Conf. on *Nuclear physics,* Tokyo, and to be published.
[15]) W. Kohl, D. Kolb and I. Giese, Z. Physik, in press.
[16]) Th. Lindblad, Nukleonika 22 (1977) 1065.
[17]) W. J. Ockels, Z. Physik, to be published.

PRINTED IN BELGIUM BY CEUTERICK, LOUVAIN